ORACM: Online region-based active contour model

M. Fatih Talu *

Computer Engineering Department, Inonu University, 44280 Malatya, Turkey

A B S T R A C T

A new online region-based active contour model (ORACM) is proposed in this paper. The classical geodesic active contour (GAC) model has only local segmentation property, although the Chan–Vese (C–V) model possesses global. An up-to-date active contour model (ACM with SBGFRLS) proposed in Zhang, Zhang, Song, and Zhou (2010) both has the properties of global/local segmentation and incorporates the GAC and the C–V models to raise active contours' performance on image segmentation. However it has two major disadvantages. First, it deforms the active contour model just using the gradient of current level set iteratively and so works too slowly. Second, it needs a parameter α which plays major impact on the results and to be tuned according to input images. The proposed model ORACM eliminates these two disadvantages by using a new binary level set formula and a new regularization operation such as morphological opening and closing. Without changing segmentation accuracy, ORACM requires no parameter and less time over the traditional ACMs. Experiments on synthetic and real images demonstrate that the computational cost of ORACM with the morphological operations is 3.75 times less than the traditional ACMs on average.

© 2013 Elsevier Ltd. All rights reserved.

1. Introduction

Robust and fast image segmentation step has a major impact on results of the applications of consumer (Subašić, Lončarić, & Heđi, 2012) and medical image processing (Lai & Chang, 2009; Vard, Monadjemi, Jamshidi, & Movahhedinia, 2011). Numerous segmentation techniques have been proposed, among which the active counter model (ACM) (Zhang et al., 2010; Chan & Vese, 2001; Caselles, Kimmel, & Sapiro, 1997; Tseng, Hsieh, & Jeng, 2009) is one of the most successful methods. The main idea of ACM is to delineate an object outline from a noisy image by minimizing an energy associated to a sum of an internal and external energy. The existing ACM methods can be classified into two categories as region-based (Chan & Vese, 2001; Li, Kao, Gore, & Ding, 2007; Lie, Lysaker, & Tai, 2006; Zhang et al., 2010) and edge-based (Brox, Rousson, Deriche, & Weickert, 2010; Caselles et al., 1997; Osher & Fedkiw, 2002; Tseng et al., 2009) models. Region-based approaches derive a counter representation from a segmentation of the image into well-defined regions, while edge-based methods takes into account the fact that boundary points can be characterized by a differential property as image gradient and a counter representation be fitted to the boundary points. In the region-based approach, first a user defined curve is determined and then an energy minimization algorithm is used to deform the active counter model until it fits objects boundaries. In the edge-based approach, a pixel belongs

to the boundary if it passes a numerical test such as local maximum of the image gradient (Ronfard, 1994).

Possessing the many advantages over the edge-based approaches, the region-based approaches are generally preferred. One advantage is that the region-based models utilize the statistical information inside and outside the contour to update the active contour. So they are less sensitive to noise and have better performance for images with weak edges or without edges. Second, they try to detect the exterior and interior boundaries simultaneously and they are significantly less sensitive to the location of initial contour (Zhang et al., 2010).

Due to encoding many advantages such as intrinsic, parameter free and implicit, the level set methods (Brox et al., 2010; Lie et al., 2006; Osher & Fedkiw, 2002; Zhang et al., 2010) provide a direct way to estimate the geometric properties of the evolving structure, can change the topology. The level set methods can be used to efficiently address the problem of curve/surface propagation in an implicit manner. In conclude they provide a very convenient framework together with the region-based active contour models to address image segmentation problem.

In this paper, an online region-based active contour model (named as ORACM) using a new level set formulation is proposed. In brief, when compared to the traditional ACMs, the advantages of ORACM can be expressed as providing less time without changing accuracy ratio and parameter free.

The paper is organized as follows: In Section 2, the classical ACMs are reviewed. Section 3 describes the formulation of ORACM and how to construct the region-based ACM. The advantages of

---

* Tel.: +90 5544907043; fax: +90 4223410046.
  E-mail addresses: fatihtalu@gmail.com, fatih.talu@inonu.edu.tr

ORACM over the GAC, C–V and ACM with SBGFRLS models are also discussed in this section. Section 4 validates ORACM by extensive experiments on synthetic and real images. Knowledge about implementation is given in Section 5. In Section 6, limitations of the ORACM and future work are represented. Section 7 concludes the paper.

2. The GAC, C–V and ACM with SBGFRLS models

2.1. The GAC model

The GAC model is an edge based active contour model for the detection of the object boundaries which is based on active contours evolving in time according to intrinsic geometric measures of the image (Caselles, Kimmel, & Sapiro, 1995; Caselles et al., 1997). In the GAC model, the following level set formula is used.

$$\frac{\vartheta\phi}{\vartheta t} = g|\nabla\phi|\left(\text{div}\left(\frac{\nabla\phi}{|\nabla\phi|}\right) + \alpha\right) + \nabla g.\nabla\phi \tag{1}$$

where $\nabla\phi$ is the curvature approximation of the level set ϕ and α is the balloon force, which controls the contour shrinking or expanding. The GAC model has been extensively employed in pattern recognition (Chen, Zhou, Wang, & Yang, 2006). The GAC model has some major disadvantages. One of them is to have a high computational cost due to the need to compute the gradient ∇g of curvature approximation $\nabla\phi$ of the current level set ϕ in each iteration. For this, firstly the first and second derivatives of ϕ by using the central differences are computed, and then the gradient and curvature approximation are computed as follows:

$$\left.\begin{array}{ll} \phi_x = \phi * G_x, & G_x = I(x+1, y) - I(x-1, y) \\ \phi_y = \phi * G_y, & G_y = I(x, y+1) - I(x, y-1) \end{array}\right\} \text{first derivatives} \tag{2}$$
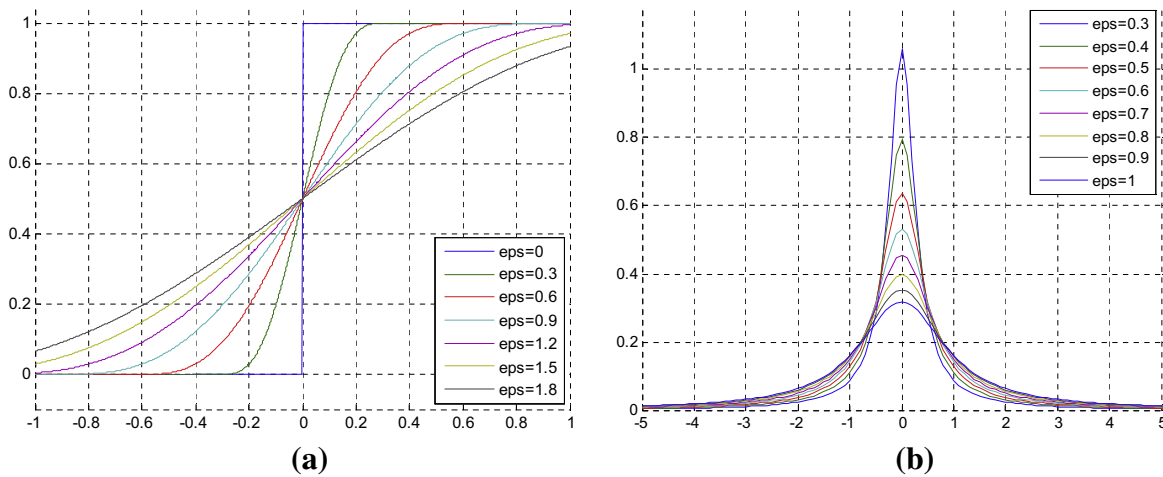

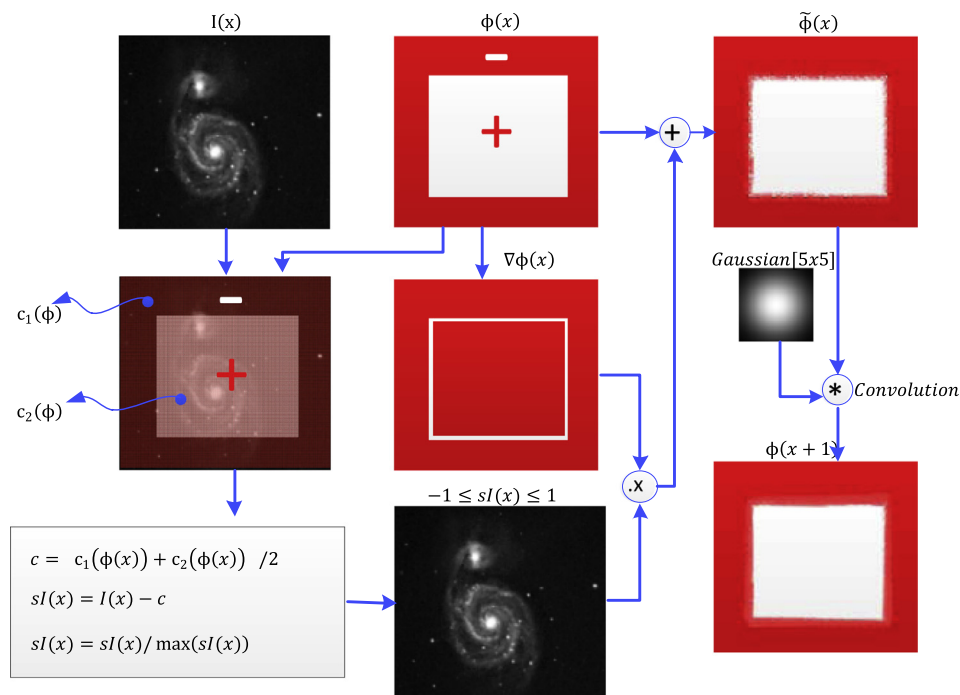**Fig. 1.** (a) The Heaviside function (b) The Dirac function.

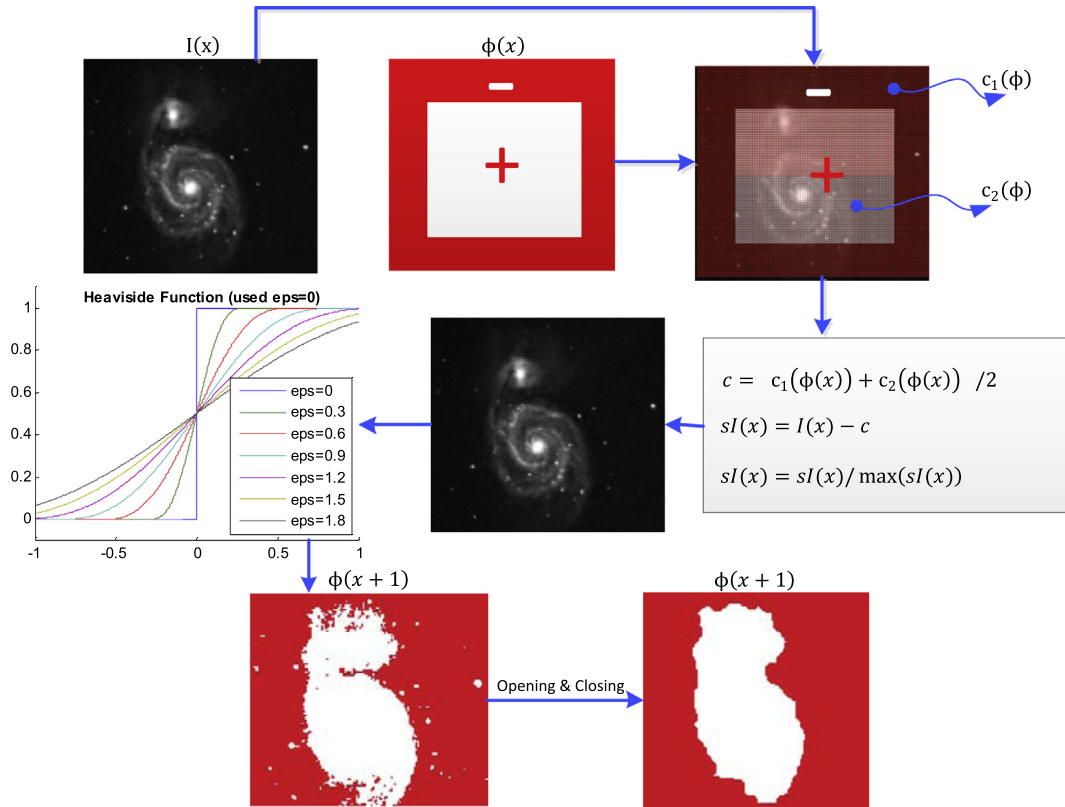**Fig. 2.** An iteration of the ACM with SBGFRLS.

I(x)

$\phi(x)$

$c_1(\phi)$

$c_2(\phi)$

Heaviside Function (used eps=0)

eps=0
eps=0.3
eps=0.6
eps=0.9
eps=1.2
eps=1.5
eps=1.8

$$c = \quad c_1(\phi(x)) + c_2(\phi(x)) \quad /2$$

$$sI(x) = I(x) - c$$

$$sI(x) = sI(x)/\max(sI(x))$$

$\phi(x+1)$

$\phi(x+1)$

Opening & Closing

Fig. 3. An iteration of ORACM.

Iteration: 0	Iteration:1	Iteration:2	Iteration:3	Iteration:4	Iteration:5	Iteration:6
Toa:9646, Obj:1	Toa:6051, Obj:49	Toa:3896, Obj:43	Toa:3177, Obj:24	Toa:2868, Obj:19	Toa:2722, Obj:22	Toa:2651, Obj:28
Toa:9646, Obj:1	Toa:6238, Obj:1	Toa:4046, Obj:1	Toa:3437, Obj:1	Toa:3156, Obj:2	Toa:3117, Obj:2	Toa:3055, Obj:2
Toa:9646, Obj:1	Toa:14318, Obj:1	Toa:13651, Obj:1	Toa:13324, Obj:1	Toa:12995, Obj:1	Toa:12662, Obj:3	Toa:12336, Obj:3
Toa:4959, Obj:1	Toa:4959, Obj:1	Toa:4958, Obj:1	Toa:4956, Obj:1	Toa:4952, Obj:1	Toa:4951, Obj:1	Toa:4952, Obj:1

Fig. 4. The segmentation results of the ACMs.

0th iteration, the total area of the object:0 | 10th iteration, the total area of the object:29289 | 20th iteration, the total area of the object:25646

30th iteration, the total area of the object:22502 | 40th iteration, the total area of the object:19538 | 50th iteration, the total area of the object:17334

60th iteration, the total area of the object:16306 | 70th iteration, the total area of the object:14828 | 80th iteration, the total area of the object:13328

90th iteration, the total area of the object:11110 | 100th iteration, the total area of the object:7139 | 110th iteration, the total area of the object:5237

(a)

(b)

0th iteration, the total area of the object:32400 | 1th iteration, the total area of the object:16971

2th iteration, the total area of the object:12905 | 3th iteration, the total area of the object:8529

4th iteration, the total area of the object:5685 | 5th iteration, the total area of the object:5178

6th iteration, the total area of the object:5062 | 7th iteration, the total area of the object:5062
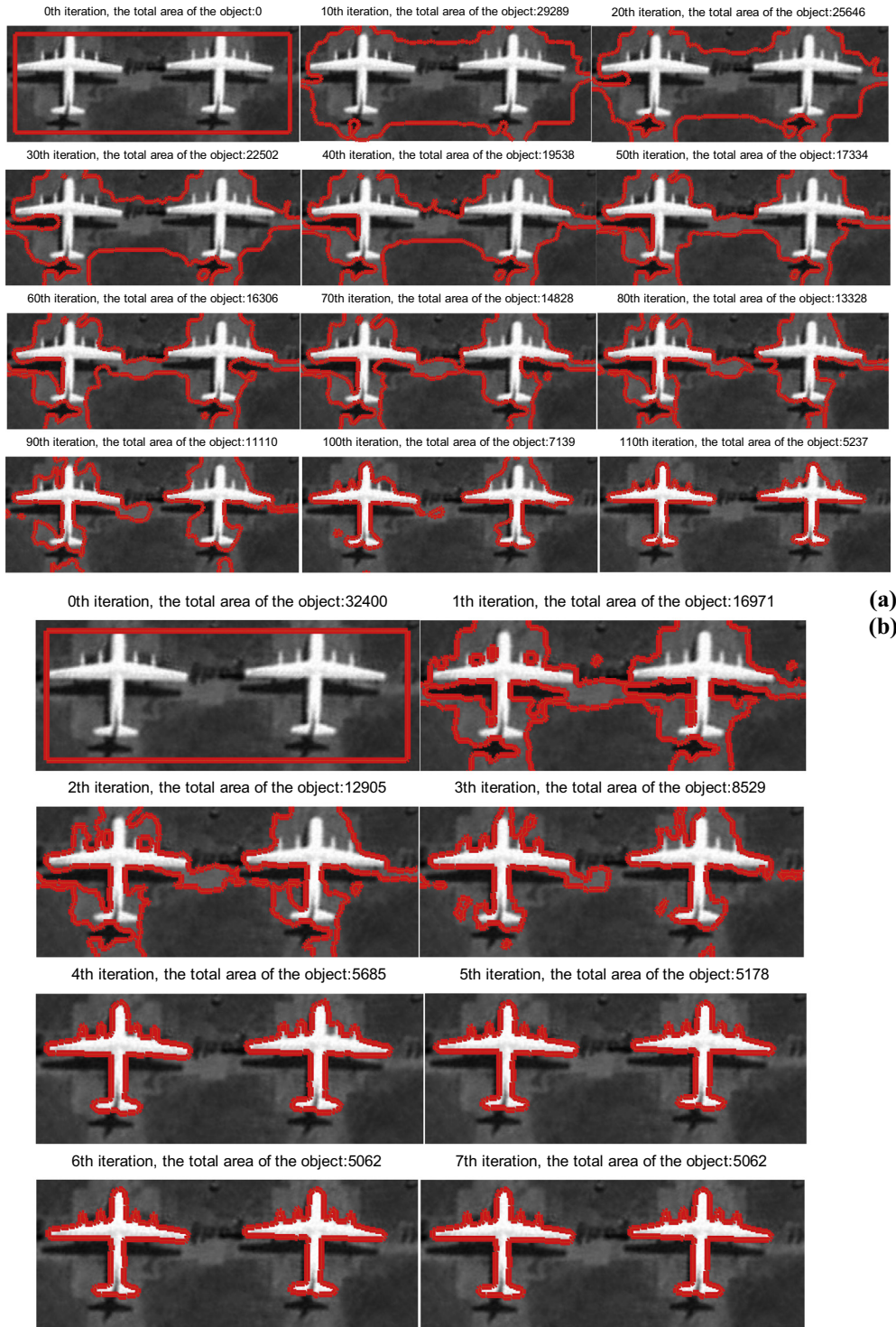
Fig. 5. Global segmentation results of (a) the ACM with SBGFRLS ($\alpha = 10$) (b) ORACM.

$$
\left.\begin{array}{ll}
\phi_{xx} = \phi * G_{xx}, & G_{xx} = I(x+1,y) + I(x-1,y) - 2*I(x,y) \\
\phi_{yy} = \phi * G_{yy}, & G_{yy} = I(x,y+1) + I(x,y-1) - 2*I(x,y) \\
\phi_{xy} = \phi * G_{xy}, & G_{xy} = I(x+1,y) + I(x-1,y) - 2*I(x,y)
\end{array}\right\} \text{second derivatives} \tag{3}
$$

$$
\nabla g = \sqrt{\phi_x^2 + \phi_y^2} \left.\right\} \text{gradient} \tag{4}
$$

$$
\nabla \phi = \frac{\phi_{xx}.\phi_{yy} - \phi_{xy}^2}{\left(1 + \phi_x^2 + \phi_y^2\right)^2} \left.\right\} \text{curvature} \tag{5}
$$

Because of performing all these calculations in each iteration, the GAC model has the expense of longer calculation times. The other disadvantage is that the GAC model is based on gradient and curvature to detect boundary, in which only local information of
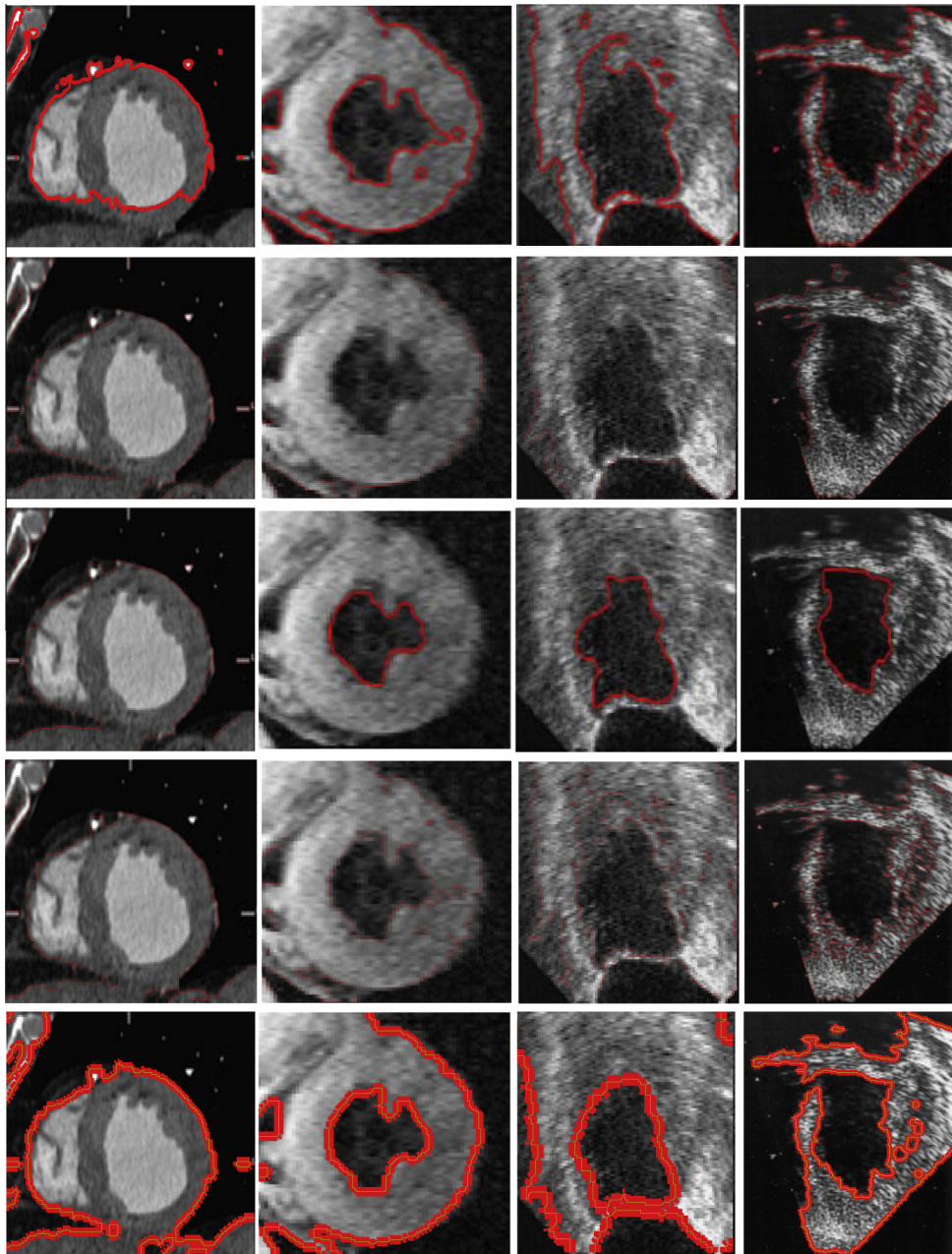
Fig. 6. Segmentation results of ACMs in medical images.

boundary is used. Because of the local attributes and the dependence on gradient, the GAC model is heavily affected by noise inputs.

2.2. The C–V model

For a given image I in domain φ, the level set formulation of the C–V method (Chan & Vese, 2001), which is based on Mumford Shah segmentation techniques (Mumford & Shah, 1989), is as follows:

$$\begin{cases} C = \{x \in \varphi : \phi(x) = 0\} \\ \text{inside}(C) = \{x \in \varphi : \phi(x) > 0\} \\ \text{outside}(C) = \{x \in \varphi : \phi(x) < 0\} \end{cases} \quad (6)$$

where $\phi(x)$ denotes level set and C shows active curve in image. To be able to update the zero level set $(\phi(x) = 0)$, the C–V method

calculates the corresponding variation level set formulation given as follows:

$$\frac{\vartheta \phi}{\vartheta t} = \delta(\phi) \left[\mu \nabla \left(\frac{\nabla \phi}{|\nabla \phi|} \right) - \upsilon - \lambda_1 (I - c_1)^2 + \lambda_2 (I - c_2)^2 \right] \quad (7)$$

where μ controls the smoothness of the level set, υ increases the propagation speed, λ_1 and λ_2 are fixed parameters, which control the image data driven force inside and outside the contour. ∇ is the gradient operator. $H(\phi)$ and $\delta(\phi)$ are the Heaviside function and the Dirac function as shown in Fig. 1(a) and (b), respectively.

In Eq. (7), c_1 and c_2 are two constants which are the average intensities inside and outside the contour, respectively and calculated as follows:

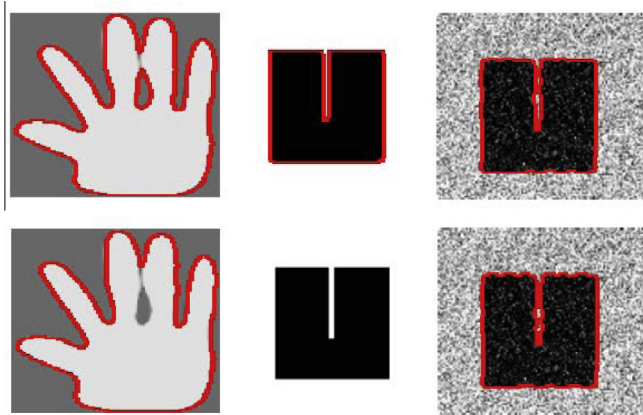$$c_1(\phi) = \frac{\int^I (x).H(\phi)dx}{\int^H (\phi)dx} \quad (8)$$

Fig. 7. The segmentation results by ORACM and the ACM with SBGFRLS model on synthetic images.

$$c_2(\phi) = \frac{\int^I(x).(1 - H(\phi))dx}{\int(1 - H(\phi))dx} \tag{9}$$

The C–V model has two major disadvantages. First, as similar to the GAC model, it also needs to calculate the curvature approximation $\nabla\phi$, which tends to high computational expense. Second, it possesses only global segmentation property which can segment the desired object with a proper initial contour. It cannot extract the interior contour without setting the initial one inside the object and fails to extract all the objects.

2.3. The ACM with SBGFRLS model

Another region based active contour method is the ACM with SBGFRLS (Zhang et al., 2010), in which a user-defined active contour is determined at the initialization step and then it is continuously updated by a region-based signed pressure function (SPF) defined as follows:

$$\text{spf}(I(x,y)) = \frac{I(x,y) - \frac{c_1+c_2}{2}}{\max\left(\left|I(x,y) - \frac{c_1+c_2}{2}\right|\right)} \tag{10}$$

where c_1 and c_2 are defined in Eqs. (8) and (9), respectively. Unlike the C–V method in the calculation of c_1 and c_2, the ACM with SBGFRLS uses the α Heaviside function only with eps = 0. The SPF function modulates the signs of the pressure force inside and outside the region of interest so that the contour shrinks when outside the object, or expands when inside the object. In addition, the ACM
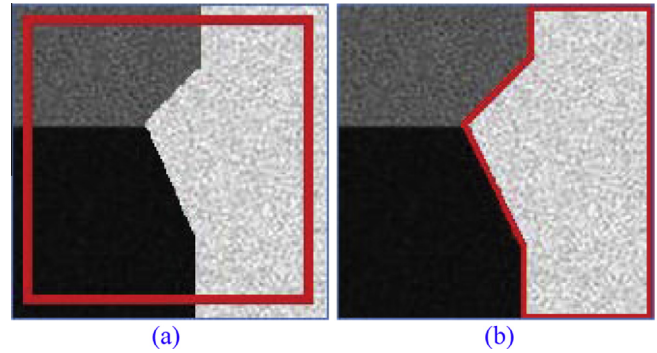

Fig. 8. (a) The initial level set (b) Segmentation result of ORACM.

with SBGFRLS uses the corresponding variation level set formulation given as follows:

$$\frac{\vartheta\phi}{\vartheta t} = \text{spf}(I(x)).\alpha.|\nabla\phi| \tag{11}$$

where α is a constant and controls the speed of level set update. The major disadvantage of the ACM with SBGFRLS is that although plays major impact on the result, it must be tuned according to image. This situation makes the use of the ACM with SBGFRLS difficult on different images and impossible on real-time video images. Its other disadvantage is slowness. $|\nabla\phi|$ denotes the gradient of the level set function and is calculated as defined at Eq. (4). Using $|\nabla\phi|$ at the level set formulation propagates the result of the SPF function only on boundary of the level set function. In this case the boundary of level set is only updated, which causes slowness. For better comprehension, an iteration of the ACM with SBGFRLS is illustrated in Fig. 2.

3. The proposed method (ORACM)

ORACM is a region based active contour method which both requires no parameter and less time without changing segmentation accuracy over the traditional ACMs. It performs a sort of block thresholding process in each iteration. This tresholding process produces rigid boundaries and many small particles, does not belong to the object. To remove these small particles and to obtain smooth and proper object contour, the opening and closing morphological operations are applied respectively.

As similar to the ACM with SBGFRLS, ORACM also uses a user-defined active contour at the initialization step and then continuously updates it. The level set function is shown as $\varphi(x)$ in Fig. 3

Table 1
The comparison results for the elapsed time (sec) and the number of iterations.

	ORACM₁		ORACM₂		ACM with SBGFRLS		C–V	
	Time	Iteration	Time	Iteration	Time	Iteration	Time	Iteration
Img1	0.365	**8**	**0.284**	9	0.915	73	66.451	1932
Img2	**0.037**	**5**	0.170	5	0.240	46	47.550	3493
Img3	**0.027**	**2**	0.078	2	0.026	5	0.158	23
Img4	**0.051**	5	0.111	**3**	0.090	40	1.331	187
Img5	**0.051**	**7**	0.330	7	0.687	66	20.220	1169
Img6	**0.020**	4	0.057	**3**	0.120	77	80.983	15049
Img7	0.267	**5**	**0.163**	6	4.120	266	19.426	475
Img8	**0.039**	**7**	0.155	7	0.842	93	7.094	289
Img9	**0.026**	7	0.103	**5**	0.179	44	0.234	19
Img10	**0.020**	11	0.107	**6**	0.027	40	0.096	48
Img11	**0.019**	**4**	0.092	5	0.014	14	0.227	74
Img12	**0.021**	4	0.057	**3**	0.029	18	0.729	130
Img13	**0.022**	7	0.129	7	0.161	90	0.754	133

and initialized to constants, which have different signs such as −1 and +1 inside and outside the contour. Unlike the ACM with SBGFRLS, ORACM uses a simple and efficient level set updating formulation as given follows:

$$\frac{\vartheta \phi}{\vartheta x} = H(\mathrm{spf}(I(x))).\phi(x) \tag{12}$$

where $H(.)$ is the Heaviside function with as is shown in Fig. 1(a)), spf(.) is the signed pressure function defined at Eq. (10), $I(x)$ denotes an input image and $\phi(x)$ denotes the current level set. The significance of Eq. (12) and the differences from the level set formulations of the traditional ACMs can be explained as follows:

- Unlike Eq. (11), it does not require a parameter α which is needed to be tuned according to input images. This contribution gives ORACM the property of being an algorithm, needs no parameter.
- Unlike Eqs. (1) and (7), it does not need to calculate the curvature approximation $\nabla \phi$ which tends to the expense of longer calculation times.
- Due to not having mathematical complexity, it is easily understandable.
- Unlike Eq. (11), it uses directly current level set $\phi(x)$ instead of $|\nabla \phi|$. This change propagates the result of the SPF on the entire current level set $\phi(x)$ instead of its boundary. This situation leads to an increase in the current level set update rate without affecting the accuracy of the algorithm. For better comparison with the ACM with SBGFRLS, an iteration of ORACM is illustrated in Fig. 3 from which we can easily see how quickly the current level set with a square-shaped turns into the shape of object in image only at the end of an iteration. Some examples to show better the effect of this change will be given (see Fig. 4 in Section 5 for example).

Another difference between the ACM with SBGFRLS and ORACM lies in the smoothing step of the level set function. To smooth updated level set, a Gaussian filter is used at each iteration of the ACM with SBGFRLS. However, ORACM uses a simple morphological opening and closing processes instead of Gaussian smoothing. As we can see from Fig. 4, after the updating process of level set, many small particles, which do not belong to the object, can occur. All these particles can be eliminated by the opening process and the smooth boundaries of objects can be obtained by closing.

4. Implementation

To make an accurate comparison, in the all experimentations performed in this study, two parameters, which are any input image and a used defined initial mask, were used as common for all the ACMs. In addition, the ACM with SBGFRLS needs one more parameter, which is (the speed of level set update), given at Eq. (11). The C–V needs two more parameter μ and υ defined at Eq. (7).

To make an accurate comparison of the performances, the stopping criterion in all the ACMs is set as internal and external energy change of object as follows:

$$\int H(\phi(t)) - \int H(\phi(t-1)) = 0 \tag{13}$$

where $H(\phi(t))$ and $H(\phi(t-1))$ denote the total energy densities at time t and $t-1$ respectively.

All of the ACMs are implemented in Matlab 2011b on a PC with 2.9-GHz Intel(R) Core(TM)2 Duo CPU and 4 GB RAM. Matlab codes of all algorithms and sample images can be downloaded as a single file from http://iys.inonu.edu.tr/webpanel/dosyalar/1348/file/OnlineSeg.rar (xxxx).

5. Experimental results

The first experiment was performed to understand more the effect of the morphological process in ORACM in comparison with the classical ACMs. Fig. 4 shows the segmentation results of OR-ACM and the classical methods for the first six iterations and the green[1] curve shows the boundaries of the current level set in each iteration. First row shows the results of ORACM without morphological operations. As is shown that although ORACM can detect the boundaries of object quickly, the result has many small particles and the active contour is not smooth. To remove small objects and to smooth the active contour, the opening and closing morphological operations are used respectively. These two operations performed sequentially are commonly used in computer vision and image processing for noise removal and smoothing. Second row shows the results of ORACM with morphological operations. As can be seen easily from these results, ORACM is able to detect soft object boundaries after only six iterations. Third and four rows show the results of the ACM with SBGFRLS (the parameter α = 25) and the C–V methods, respectively. The results show that the classical ACMs update the active contour slowly. In addition, the value of total area in green curves is given on image in each iteration. Note that, although this value surprisingly fluctuates in the classical ACMs, it steadily decreases in ORACM.

The second experiment was performed to understand more speeds of the ACM with SBGFRLS and ORACM in a global segmentation problem. Fig. 5(a) demonstrates the segmentation results of the ACM with SBGFRLS with α = 10 for an image with two planes. As shown, it cannot detect the boundaries of the planes after 110 iterations. Fig. 5(b) demonstrates the results of ORACM for similar image. Note that, without the need of any parameter, ORACM correctly detects the boundaries of the planes after only seven iterations. This acceleration comes from the use of the proposed level set formulation defined in Eq. (12).

In the Fig. 6, it is aimed to have a better understanding of the segmentation accuracy of the classic ACMs and ORACM on four different noisy medical images. The first and second columns show two magnetic resonance images of the left ventricle and of a human heart, and the right two columns show two ultrasound images of the same organ of a human heart. The first row shows the segmentation results of the C–V method which fails to extract inner region contours in some images. The second and third rows show the segmentation results of the ACM with SBGFRLS, which fails to extract contours of all the objects in different areas. The fourth and fifth row shows the results of ORACM with and without the morphological process, respectively. Note that the results obtained for the first and third images by ORACM are quite different, results from consideration of small particles in the algorithm. Consequently, looking by the results in the fifth row we can say that, OR-ACM with the morphological process could accurately extract the boundaries of all objects.

Fig. 7 demonstrates the segmentation accuracy of the ACM with SBGFRLS and ORACM on the synthetic images. The segmentation results by ORACM are shown in first row. The segmentation results by the ACM with SBGFRLS (α = 25) are shown in second row. Note that the ACM with SBGFRLS cannot detect both the inner region of the hand at the first column and simple square object, whereas ORACM can accurately detect inner and outer regions of all synthetic images.

Table 1 represents the comparison results for the elapsed time and the number of iterations obtained by the ACMs for 13 different images (can be downloaded from http://iys.inonu.edu.tr/webpanel/dosyalar/1348/file/OnlineSeg.rar (xxxx) used in this study. For

---

[1] For interpretation of color in Fig. 4, the reader is referred to the web version of this article.

all ACMs, the elapsed time shows the time from the beginning of algorithm to the absence of any change in current level set. OR-ACM1 and ORACM2 denote ORACM with or without the morphological operations respectively. As shown in the first two colons in Table 1, using these operations causes some slowness. Surprisingly, in some images such as Img2 and Img8, $ORACM_1$ is slower than $ORACM_2$ although the iteration number of $ORACM_2$ is high. This is because the small particles in the results of $ORACM_1$ according to intensity distribution of input image. Because these particles may lead to a long-term change of the level set, the completion of the algorithm takes longer time. However, in the all other images, $ORACM_1$ is faster than $ORACM_2$. In addition, the classical ACMs consume excessively high time. The ACM with SBGFRLS is the best method in conventional methods. However, it can be shown that the average computational cost of ORACM is approximately 3.75 times less than the ACM with SBGFRLS. In addition, the iteration number of the classical ACMs is extremely high in comparison with ORACM. ORACM is constantly changing according to intensity distributions of the input images. The obtained minimum time and iteration values for each image in Table 1 are represented as bold.

6. Limitation of the model and future work

Despite of providing a significant improvement in terms of speed over the traditional ACMs, ORACM has a major disadvantage that it supports only bimodal segmentation of piecewise constant intensity distribution. This deficiency limits the application of ORACM to problems that satisfy these constraints. To exemplify, Fig. 8 shows an example where ORACM would fail to provide an appropriate segmentation. In Fig. 8(a), an image with three different colors, in which is exhibited a very high level of inhomogeneity and the initial contour of ORACM are shown. Fig. 8(b) represents the final segmentation result of ORACM. As shown, the obtained result is not true.

For future study, the extension of ORACM will be investigated to multi-phase image segmentation by introducing more than two labels to the model.

7. Conclusion

In this paper, we proposed an online region-based active contour model named as ORACM which is implemented by a new level set formulation, which does not require any extra parameter to be tuned according to input images. The proposed method can decrease the computational complexity without changing the accuracy of the image segmentation process. In addition, it can accurately segment all inside and outside object regions in medical, real and synthetic images within holes, complex background, weak edges, and highly noise. These important contributions over the classical methods such as the GAC, C–V and ACM with SBGFRLS can provide the proposed method to be favored especially in online segmentation applications. However, the proposed method supports only bimodal segmentation of piecewise constant intensity distribution. Extensive experiments on synthetic and real images demonstrated the advantages according to accuracy and elapsed time of the proposed method over the classical ACMs having the properties of local and global segmentation.

Appendix A. Supplementary data

Supplementary data associated with this article can be found, in the online version, at http://dx.doi.org/10.1016/j.eswa.2013.05.056.

References

Brox, T., Rousson, M., Deriche, R., & Weickert, J. (2010). Colour, texture, and motion in level set based segmentation and tracking. *Image and Vision Computing, 28*, 376–390.

Caselles, V., Kimmel, R., & Sapiro, G. (1995). Geodesic active contours. In *Processing of IEEE international conference on computer vision* (pp. 694–699). Boston, MA.

Caselles, V., Kimmel, R., & Sapiro, G. (1997). Geodesic active contours. *International Journal of Computer Vision, 22*(1), 61–79.

Chan, T., & Vese, L. (2001). Active contours without edges. *IEEE Transaction on Image Processing, 10*(2), 266–277.

Chen, L., Zhou, Y., Wang, Y., & Yang, J. (2006). GACV: Geodesic-Aided C–V Method. *Pattern Recognition, 39*, 1391–1395.

<http://iys.inonu.edu.tr/webpanel/dosyalar/1348/file/OnlineSeg.rar>. 01/05/2013.

Lai, C.-C., & Chang, C.-Y. (2009). A hierarchical evolutionary algorithm for automatic medical image segmentation. *Expert Systems with Applications, 36*(1), 248–259.

Li, C. M., Kao, C., Gore, J., & Ding, Z. (2007). Implicit active contours driven by local binary fitting energy. In *IEEE Conference on Computer Vision and, Pattern Recognition*.

Lie, J., Lysaker, M., & Tai, X. C. (2006). A binary level set model and some application to Munford–Shah image segmentation. *IEEE Transaction on Image Processing, 15*, 1171–1181.

Mumford, D., & Shah, J. (1989). Optimal approximations by piecewise smooth functions and associated variational problems. *Communication on Pure and Applied Mathematics, 42*(5), 577–685.

Osher, S. J., & Fedkiw, R. P. (2002). *Level Set Methods and Dynamic Implicit Surfaces*. 0-387-95482-1. Springer-Verlag.

Ronfard, R. (1994). Region-based strategies for active counter models. *International Journal of Computer Vision 1, 3*(2), 229–251.

Subašić, M., Lončarić, S., & Heđi, A. (2012). Segmentation and labeling of face images for electronic documents. *Expert Systems with Applications, 39*(5), 5134–5143.

Tseng, C. C., Hsieh, J. G., & Jeng, J. H. (2009). Active contour model via multi-population particle swarm optimization. *Expert Systems with Applications, 36*(3 Part 1), 5348–5352.

Vard, A. R., Monadjemi, A. M., Jamshidi, K., & Movahhedinia, N. (2011). Fast texture energy based image segmentation using directional Walsh–Hadamard transform and parametric active contour models original research article. *Expert Systems with Applications, 38*(9), 11722–11729.

Zhang, K., Zhang, L., Song, H., & Zhou, W. (2010). Active contours with selective local or global segmentation: A new variational approach and level set method. *Image and Vision Computing, 28*, 668–676.